ACS Catalysis

pubs.acs.org/acscatalysis

Research Article

Flame Synthesis of Cu/ZnO–CeO_2 Catalysts: Synergistic Metal–Support Interactions Promote CH_3OH Selectivity in CO_2 Hydrogenation

Jiadong Zhu, Diana Ciolca, Liang Liu, Alexander Parastaev, Nikolay Kosinov, and Emiel J. M. Hensen*

Cite This: *ACS Catal.* 2021, 11, 4880–4892

Read Online

ACCESS | Metrics & More | Article Recommendations | Supporting Information

ABSTRACT: The hydrogenation of CO_2 to CH_3OH is an important reaction for future renewable energy scenarios. Herein, we compare Cu/ZnO, Cu/CeO_2, and Cu/ZnO–CeO_2 catalysts prepared by flame spray pyrolysis. The Cu loading and support composition were varied to understand the role of Cu–ZnO and Cu–CeO_2 interactions. CeO_2 addition improves Cu dispersion with respect to ZnO, owing to stronger Cu–CeO_2 interactions. The ternary Cu/ZnO–CeO_2 catalysts displayed a substantially higher CH_3OH selectivity than binary Cu/CeO_2 and Cu/ZnO catalysts. The high CH_3OH selectivity in comparison with a commercial Cu–ZnO catalyst is also confirmed for Cu/ZnO–CeO_2 catalyst prepared with high Cu loading (~40 wt %). In situ IR spectroscopy was used to probe metal–support interactions in the reduced catalysts and to gain insight into CO_2 hydrogenation over the Cu–Zn–Ce oxide catalysts. The higher CH_3OH selectivity can be explained by synergistic Cu–CeO_2 and Cu–ZnO interactions. Cu–ZnO interactions promote CO_2 hydrogenation to CH_3OH by Zn-decorated Cu active sites. Cu–CeO_2 interactions inhibit the reverse water–gas shift reaction due to a high formate coverage of Cu and a high rate of hydrogenation of the CO intermediate to CH_3OH. These insights emphasize the potential of fine-tuning metal–support interactions to develop improved Cu-based catalysts for CO_2 hydrogenation to CH_3OH.

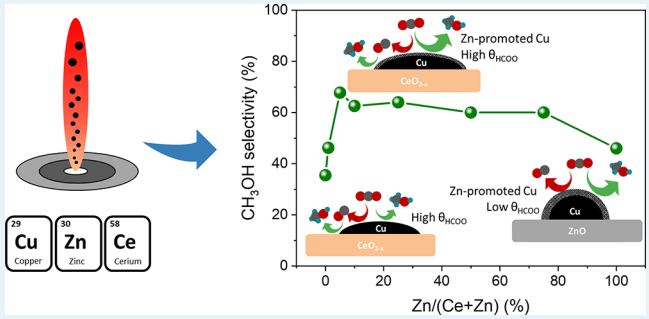

KEYWORDS: *CO_2 hydrogenation, methanol, ceria, metal–support interaction, flame spray pyrolysis*

1. INTRODUCTION

Methanol is an important commodity in the current chemical industry and expected to play a central role in the transition toward a sustainable economy as a platform chemical for the production of energy carriers and chemicals.[1] Modern industrial methanol production is based on the conversion of synthesis gas using Cu/ZnO/Al_2O_3 catalysts operated at elevated temperature (200–300 °C) and pressure (50–100 bar).[2] Catalytic conversion of CO_2 to methanol ($CO_2 + 3H_2 \rightarrow CH_3OH + H_2O$) using green hydrogen generated from sustainable energy sources has recently attracted significant attention.[3,4] This approach allows the reuse of the greenhouse gas CO_2 for the production of fuels and chemicals using methanol as a platform.[4,5] Although Cu/ZnO/Al_2O_3 catalysts are active for CO_2 hydrogenation to CH_3OH, there are several problems with respect to its practical implementation. A major drawback lies in the high activity in the reverse water–gas shift (rWGS, $CO_2 + H_2 \rightarrow CO + H_2O$) reaction of Cu/ZnO/$Al_2O_3$ catalysts. The WGS reaction ($CO + H_2O \rightarrow CO_2 + H_2$) is important for methanol synthesis from synthesis gas over Cu/ZnO/Al_2O_3 catalysts because the main reaction pathway involves direct hydrogenation of CO_2.[6–8] However, a high rWGS activity is undesirable for CH_3OH synthesis from CO_2, because the production of CO byproduct decreases CH_3OH selectivity and H_2 utilization efficiency.[8] The formation of a large amount of water byproduct during CO_2 hydrogenation in comparison to synthesis gas hydrogenation poses another challenge to catalyst stability, as water can accelerate the deactivation of Cu/ZnO/Al_2O_3 catalysts.[9–12]

A strategy to improve Cu–ZnO-based catalysts for CO_2 hydrogenation to methanol is to replace Al_2O_3 by other supports. ZrO_2, for instance, has been widely investigated in this respect.[13–16] CeO_2 is another promising support material to promote CO_2 conversion.[17] CeO_2 is more basic and less hydrophilic than Al_2O_3, which can be beneficial for CH_3OH productivity and catalyst stability, respectively.[18,19] CeO_2 interacts strongly with Cu, which may improve dispersion and resistance against sintering of the Cu particles.[20] While

Received: January 11, 2021
Revised: March 23, 2021
Published: April 6, 2021

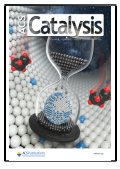

binary Cu/CeO_2 catalyst is known for its high activity in CO hydrogenation to methanol,[21,22] a recent study showed that it is also promising for CO_2 hydrogenation to methanol.[23] The influence of CeO_2 addition to Cu−ZnO-based catalysts has been investigated as well.[18,24−28] Bonura et al. used a reverse co-precipitation method to prepare promoted Cu-based catalysts under ultrasonic conditions and found that CeO_2 was a better promoter for CH_3OH formation than ZrO_2 in CO_2 hydrogenation.[24] Gao et al. prepared a series of promoted Cu−ZnO-based catalysts from hydrotalcite-like precursors[25] and showed that the copper surface area and the fraction of strongly basic sites increased after CeO_2 addition, resulting in a higher CO_2 conversion and CH_3OH selectivity than the unpromoted catalyst. In spite of these interesting results, a detailed structure-performance understanding of Cu−ZnO−CeO_2 catalysts in CO_2 hydrogenation to CH_3OH remains largely unaddressed.

Regarding methanol synthesis catalyst preparation, academic studies often used impregnation methods to load Cu on a support.[29,30] However, this method is limited by the relatively low Cu loading that can be achieved.[31] Co-precipitation is another often used method to prepare methanol synthesis catalysts, and it is also used to prepare commercial Cu/ZnO/Al_2O_3 catalysts.[32−34] There are, however, disadvantages associated with co-precipitation as well.[35] First, co-precipitation is time-consuming in comparison with impregnation. A washing step is required to remove the precipitation agent, which involves the use of a large amount of solvent. A promising alternative method to prepare methanol synthesis catalysts is flame spray pyrolysis (FSP), which offers advantages with respect to flexibility, speed, and scalability.[36−41] In an earlier report, Jensen et al. demonstrated that Cu/ZnO/Al_2O_3 catalysts with a relatively high specific surface area (>100 m^2/g_{cat}) can be obtained using a flame combustion method.[41] Using a two-nozzle spray pyrolysis approach, Copéret and co-workers recently prepared a series of Cu/ZrO_2 catalysts such that only the Cu particle size was varied.[37] They found that the catalysts with a smaller Cu particle size had a higher CH_3OH activity and selectivity. Tada et al. demonstrated that efficient Cu/ZrO_2 catalysts with high Cu loadings (up to 80 wt %) can be conveniently prepared by flame spray pyrolysis to convert CO_2 into methanol.[36]

In this study, we prepared three series of Cu−Zn−Ce oxide catalysts with varying support composition and Cu loading by a one-step flame spray pyrolysis (FSP) method. This method potentially allows for homogeneous mixing of different components at the nanoscale,[42,43] which is highly advantageous for elucidating the role of Cu−ZnO and Cu−CeO_2 interactions in CO_2 hydrogenation. The as-prepared Cu−Zn−Ce oxide catalysts were characterized by ICP, N_2 physisorption, TEM, STEM-EDX, XRD, TPR, and N_2O titration, confirming that well-defined catalysts with controlled Cu dispersion and Cu-support interactions can be achieved via the FSP method. The Cu−Zn−Ce oxide catalysts were evaluated for their CO_2 hydrogenation performance under the conditions of 250 °C and 30 bar. The catalytic results showed that (i) combining ZnO and CeO_2 led to a higher CH_3OH selectivity irrespective of Cu loading as compared to binary Cu/ZnO and Cu/CeO_2 catalysts and (ii) the optimized Cu−Zn−Ce oxide catalyst with high Cu loading (~40 wt %) also displayed an improved CH_3OH selectivity as compared to a commercial Cu−ZnO-based catalyst. In situ IR spectroscopy was used to gain insight into the improved CH_3OH selectivity over the ternary Cu−Zn−Ce oxide catalysts. Building upon the catalyst characterization and mechanistic studies, the improved CH_3OH selectivity of Cu−Zn−Ce oxide catalysts in CO_2 hydrogenation is discussed in the context of synergistic interactions between Cu, ZnO and CeO_2 components.

2. EXPERIMENTAL SECTION

2.1. Catalyst Preparation. Cu−Zn−Ce oxide catalysts were prepared by a single-step flame spray pyrolysis (FSP) method using a Tethis NPS10 apparatus. The catalyst precursor solution was prepared by dissolving appropriate amounts of $Cu(NO_3)_2{\cdot}3H_2O$ (99%, Sigma-Aldrich), $Zn(NO_3)_2{\cdot}6H_2O$ (99%, Sigma-Aldrich), and $Ce(NO_3)_3{\cdot}6H_2O$ (99%, Sigma-Aldrich) in a 1:1 (vol %) solvent mixture of ethanol (HPLC, Sigma-Aldrich) and 2-ethylhexanoic acid (99%, Sigma-Aldrich) at room temperature. The total metal (Cu, Zn, and Ce) concentration was 0.15 M. The precursor solution was then injected into the nozzle of the Tethis setup at a flow rate of 5 mL/min. The flame was fed with a 1.5 L/min methane flow and a 3.0 L/min oxygen flow with an additional 5.0 L/min oxygen dispersion flow around it. The resulting catalyst powder was collected from the quartz filter placed after the combustion zone. The as-prepared Cu−Zn−Ce oxide catalysts are denoted as Cu(x)/CeO_2, Cu(x)/ZnO, or Cu(x)/ZnO−CeO_2(y) where x and y, respectively, stand for Cu loading (wt %) and Zn atomic ratio in the supports (Zn/(Zn + Ce)). Additionally, a commercial Cu−ZnO-based methanol synthesis catalyst (MSC) was purchased from Alfa Aesar (no. 45776).

2.2. Catalyst Characterization. *2.2.1. Inductively Coupled Plasma Optical Emission Spectroscopy (ICP-OES).* The metal composition (Cu, Zn, and Ce) of the as-prepared catalysts was measured by ICP-OES analysis (Spectro CIROS CCD Spectrometer). To prepare samples, the Cu−Zn−Ce oxide catalysts were dissolved in 5 mL of concentrated sulfuric acid (H_2SO_4) at 150 °C under stirring for about 1 h.

2.2.2. N_2 Physisorption. The textural properties of the as-prepared catalysts were determined by measuring N_2 physisorption isotherms at −196 °C on a Micromeritics TriStar II 3020 instrument. For this purpose, about 100 mg of catalyst sample was placed into a glass sample tube and pretreated at 120 °C under a N_2 flow overnight. The Brunauer−Emmett−Teller (BET) method was used to calculate the specific surface area of the catalysts.

2.2.3. X-ray Diffraction (XRD). The crystal structure of the as-prepared catalysts was determined with a Bruker D2 Phaser diffractometer using Cu Kα radiation with a wavelength of 1.5406 Å. The XRD patters were recorded between 20−85° with a step size of 0.02° and a scan rate of 0.5 s/step.

2.2.4. Electron Microscopy (EM). The morphology of the as-prepared catalysts was studied by transmission electron microscopy (TEM) using a FEI Tecnai 20 (type Sphera) instrument operating at an acceleration voltage of 200 kV. For this purpose, appropriate amount of catalyst samples were dispersed in ethanol under ultrasonication and then deposited on holey Cu grids. The elemental distribution for reduced catalysts was determined by scanning TEM combined with energy dispersive X-ray analysis (STEM-EDX) using a FEI-cubed Cs-corrected Titan instrument operating at an acceleration voltage of 300 kV. To prepare samples, Cu−Zn−Ce oxide catalysts were reduced at 250 °C for 1 h in a flow of 10 vol % H_2 in He, followed by passivation at room temperature in a flow of 2 vol % O_2 in He. These reduced

https://doi.org/10.1021/acscatal.1c00131
ACS Catal. 2021, 11, 4880−4892

catalyst samples were then dispersed in ethanol under ultrasonication and deposited on holey Au grids.

2.2.5. Temperature-Programmed Reduction (H_2-TPR). H_2-TPR measurements were carried out using a Micromeritics AutoChem II instrument. Typically, about 50 mg of catalyst sample was held between two quartz wool layers in a quartz U-tube. The sample was pretreated at 200 °C for 1 h in a He flow of 50 mL/min prior to H_2-TPR measurement. The H_2-TPR profile was recorded by heating the sample from 40 to 700 °C at a ramp rate of 10 °C/min in a 4 vol % H_2 in He flow of 50 mL/min. The H_2 consumption during temperature ramp was monitored by a thermal conductivity detector (TCD) and the recorded signal was calibrated against a Cu/SiO_2 reference sample.

2.2.6. N_2O Titration. The surface metallic Cu sites and oxygen vacancies in the reduced Cu−Zn−Ce oxide catalysts were determined by a combined CO_2−N_2O pulsing titration method using a plug flow setup coupled with a mass spectrometer (Balzers TPG 251). This titration method allows accurate measurement of metallic Cu surface without support interference because CO_2 is used to block oxygen vacancies in the support of the reduced catalysts.[44] The detailed experimental procedures and calculations were described in a previous report.[45] In essence, one complete experiment consists of two subexperiments with sample reduction for 1 h in a 10 vol % H_2 in He flow at the beginning and sample titration using a diluted 2 vol % N_2O in a He gas mixture. The reduction temperature for catalysts with low Cu loading (x = 5) is 250 °C and for catalysts with high Cu loading (x = 45) and commercial MSC is 300 °C. Notably, the first N_2O pulse titration was carried out at 50 °C directly after the sample reduction and an extra CO_2 pulsing step at 50 °C was added between the sample reduction and the second N_2O pulse titration at 50 °C in order to block oxygen vacancies in the reduced support. The total N_2O consumption during the first N_2O titration was S_1 and during the second N_2O titration was S_2. The surface metallic Cu sites and oxygen vacancies in the reduced catalysts were calculated based on S_2 and S_1-S_2, respectively.

2.2.7. Infrared Spectroscopy. Infrared (IR) spectra were recorded on a Bruker Vertex 70v FTIR spectrometer equipped with a DTGS detector. The experiments were performed in situ by using a home-built environmental transmission IR cell. Self-supporting pellets were made by pressing approximately 12 mg of a sample in a disk with a diameter of 13 mm. Each spectrum was collected by averaging 64 scans with a resolution of 2 cm^{-1} in the 4000−1000 cm^{-1} range. The samples were reduced in 10% H_2 in He mixture at 250 °C for 1 h after heating at a rate of 5 °C/min. For CO adsorption experiments, the samples were outgassed at 250 °C prior cooling in vacuum to 40 °C. IR spectra were recorded as a function of CO partial pressure in the 0−10 mbar range. For temperature-programmed reaction (CO_2 + H_2) measurements, the samples were cooled in 10% H_2 in He reduction mixture to 50 °C following reduction and prior to exposure to the CO_2/H_2/He mixture (5:15:80, total flow 200 mL/min). The samples were heated in this reaction mixture to 250 °C at a rate of 5 °C/min, while IR spectra were recorded at intervals of 10 °C. All samples are background subtracted, and the intensity was normalized to the weight of the pellet.

2.3. Catalytic Activity Measurements. *2.3.1. CO_2 Hydrogenation.* The performance of Cu−Zn−Ce oxide and commercial MSC catalysts in CO_2 hydrogenation was evaluated at 250 °C and 30 bar in a down-flow stainless-steel reactor with an internal diameter of 4 mm. The as-prepared catalysts were pressed, crushed, and sieved to a fraction of 125−250 μm. Typically, 50 mg (for $Cu(5)/ZnO\text{-}CeO_2(y)$) or 25 mg (for $Cu(45)/ZnO\text{-}CeO_2(y)$ and commercial MSC) of catalyst diluted with 200 mg of SiC was loaded into the reactor. Prior to the reaction, the catalyst was reduced in a 10 vol % H_2 in He flow of 50 mL/min while heating to 250 °C (for $Cu(5)/ZnO\text{-}CeO_2(y)$) or 300 °C (for $Cu(45)/ZnO\text{-}CeO_2(y)$ and commercial MSC) at a rate of 5 °C/min followed by a dwell time of 1 h. The reaction was started by switching the pretreatment feed to the reaction feed at 250 °C and increasing the pressure in the reactor to 30 bar using a back-pressure regulator. The reaction feed is a gas mixture of $H_2/CO_2/N_2$ at a volumetric ratio of 3:1:1, and the total flow was 50 mL/min. The effluent gas was continuously sampled and analyzed by an online gas chromatograph (Interscience, CompactGC) equipped with Rtx-1 (FID), Rt-QBond and Molsieve 5A (TCD), and Rt-QBond (TCD) analysis sections. The measurements were taken after ca. 3 h time-on-stream, and CO_2 conversion, product selectivity, and product formation rates were calculated as follows

$$X(CO_2) = \frac{F(CO)_{out} + F(CH_3OH)_{out} + F(CH_4)_{out}}{F(CO_2)_{out} + F(CO)_{out} + F(CH_3OH)_{out} + F(CH_4)_{out}} \quad (1)$$

$$S(\text{product}) = \frac{F(\text{product})_{out}}{F(CO)_{out} + F(CH_3OH)_{out} + F(CH_4)_{out}} \quad (2)$$

$$r(\text{product}) = \frac{F(\text{product})_{out}}{V_m \times m_{cat}} \quad (3)$$

where F stands for the volumetric flow rate calculated based on N_2 internal standard using calibrated response factors and V_m for the molar volume of ideal gas at standard temperature and pressure. The CH_4 selectivity in all the measurements was very low (<1%). The turnover frequencies (TOFs) were calculated as the product (CH_3OH or CO) formation rates normalized by the amounts of surface metallic Cu sites determined by N_2O titration.

2.3.2. CO Hydrogenation. The CO hydrogenation activity of Cu−Zn−Ce oxide catalysts with low Cu loading, i.e., $Cu(5)/ZnO\text{-}CeO_2(y)$, was tested in the same catalytic setup as used for CO_2 hydrogenation. The catalyst pretreatment and reaction conditions were kept the same as done for CO_2 hydrogenation, except the CO_2 in the reaction feed being replaced by the same amount of CO. The measurements were taken after ca. 3 h time-on-stream, and CO conversion, product selectivity, and product formation rates were calculated as follows

$$X(CO) = \frac{F(CO_2)_{out} + F(CH_3OH)_{out} + F(CH_4)_{out}}{F(CO)_{out} + F(CO_2)_{out} + F(CH_3OH)_{out} + F(CH_4)_{out}} \quad (4)$$

$$S(\text{product}) = \frac{F(\text{product})_{out}}{F(CO_2)_{out} + F(CH_3OH)_{out} + F(CH_4)_{out}} \quad (5)$$

$$r(\text{product}) = \frac{F(\text{product})_{out}}{V_m \times m_{cat}} \quad (6)$$

https://doi.org/10.1021/acscatal.1c00131
ACS Catal. 2021, 11, 4880−4892

Table 1. Physicochemical Properties of Cu(x)/ZnO−CeO$_2$(y) Catalysts

catalyst	Cu loading[a] (wt %)	Zn/(Zn+Ce) atomic ratio[a]	Zn/Cu atomic ratio[a]	S_{BET}[b] (m^2/g_{cat})	D_{cu}[c] (%)	$S_{Cu(0)}$[c] (m^2/g_{cat})	$N_{Cu(0)}$[c] ($\mu mol/g_{cat}$)	N_{Ov}[c] ($\mu mol/g_{cat}$)	$R_{H2/Cu}$ ratio[d]
Cu(5)/CeO$_2$	4.8	0.00	0.00	130	62.4	19.4	472	174	1.7
Cu(5)/ZnO−CeO$_2$(0.01)	4.5	0.01	0.08	116	64.6	18.8	458	143	1.6
Cu(5)/ZnO−CeO$_2$(0.05)	4.7	0.05	0.37	128	61.1	18.5	452	206	1.6
Cu(5)/ZnO−CeO$_2$(0.10)	4.8	0.10	0.74	115	55.6	17.2	420	208	1.4
Cu(5)/ZnO−CeO$_2$(0.25)	4.7	0.26	2.17	104	52.5	15.9	388	203	1.6
Cu(5)/ZnO−CeO$_2$ (0.50)	4.7	0.51	4.97	112	46.8	14.2	347	132	1.5
Cu(5)/ZnO−CeO$_2$(0.75)	4.8	0.76	9.29	110	30.2	9.4	228	111	1.2
Cu(5)/ZnO	5.0	1.00	15.11	82	10.0	3.2	79	7	0.9
Cu(45)/CeO$_2$	38.9	0.00	0.00	91	6.8	17.2	419	138	1.1
Cu(45)/ZnO−CeO$_2$(0.25)	39.8	0.24	0.10	94	7.4	18.9	461	209	1.1
Cu(45)/ZnO−CeO$_2$(0.50)	40.1	0.51	0.25	93	7.4	19.1	466	171	1.1
Cu(45)/ZnO−CeO$_2$(0.75)	39.6	0.76	0.46	95	6.6	17.0	414	155	1.1
Cu(45)/ZnO	39.9	1.00	0.79	68	3.8	9.8	240	51	1.0
commercial MSC	45.6	1.00	0.37	89	6.5	19.0	464	67	1.0

[a]Determined from ICP-OES. [b]Determined from N_2 physisorption. [c]Determined from N_2O titration. [d]Determined from H_2-TPR.

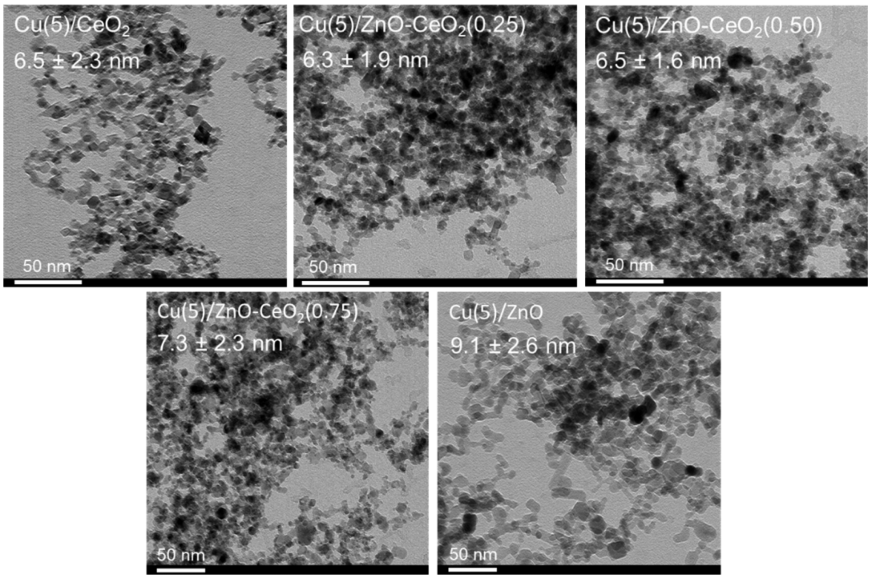

Figure 1. TEM images of FSP-prepared Cu(5)/ZnO−CeO$_2$(y) catalysts with corresponding average particle size estimations.

where F stands for the volumetric flow rate calculated based on N_2 internal standard using calibrated response factors and V_m for the molar volume of ideal gas at standard temperature and pressure. The CH_3OH selectivity in all the measurements was very high (>97%).

3. RESULTS AND DISCUSSION

Three series of Cu−Zn−Ce oxide catalysts were prepared by FSP in this study, which are catalysts with a low Cu loading and varying support composition (Cu(5)/ZnO−CeO$_2$(y)), catalysts with a high Cu loading and varying support composition (Cu(45)/ZnO−CeO$_2$(y)), and catalysts with an intermediate Cu loading and constant support composition (Cu(x)/ZnO−CeO$_2$(0.25) $5 < x < 45$). In the following sections, the series of Cu(5)/ZnO−CeO$_2$(y) and Cu(45)/Zn−CeO$_2$(y) catalysts are discussed to understand how Cu−ZnO and Cu−CeO$_2$ interactions affect Cu−Zn−Ce oxide catalysts in CO_2 hydrogenation. The results of the catalysts with intermediate Cu loadings are provided in the Supporting Information.

3.1. Characterization. The physicochemical properties of the Cu(x)/ZnO−CeO$_2$(y) catalysts (x = 5 and 45) prepared by FSP as well as the commercial MSC are listed in Table 1. The Cu loading and support composition determined by ICP-OES are close to the targeted values for all of the Cu−Zn−Ce oxide catalysts, demonstrating the reliability of FSP method in controlling catalyst composition. N_2 physisorption was used to determine the specific surface areas of the as-prepared catalysts. For the catalysts with low Cu loading (x = 5), the values range from 82 to 130 m^2/g_{cat} and the Cu/CeO$_2$ and Cu/ZnO samples exhibit, respectively, the largest and smallest surface areas. The catalysts with a high Cu loading of 45 wt % display slightly lower specific surface areas, ranging from 68 to 95 m^2/g_{cat}, compared to the catalysts with low Cu loading and the same support composition. The morphology of the Cu(5)/ZnO−CeO$_2$(y) catalysts was studied by TEM. Figure 1 shows that (i) all the samples consist of homogeneously distributed nanoparticles and (ii) the Cu/CeO$_2$ sample has a polyhedral-like morphology, whereas the Zn-containing samples are composed of rounder particles. It is also shown that the average particle size of Cu/ZnO sample (9.1 nm) was

https://doi.org/10.1021/acscatal.1c00131
ACS Catal. 2021, 11, 4880−4892

substantially larger than the size of the Ce-containing samples (6.3 to 7.3 nm), in line with the specific surface area data.

The Cu−Zn−Ce oxide catalysts with low Cu loading were stuided by XRD (Figure 2a). The Cu/CeO_2 and Cu/ZnO end

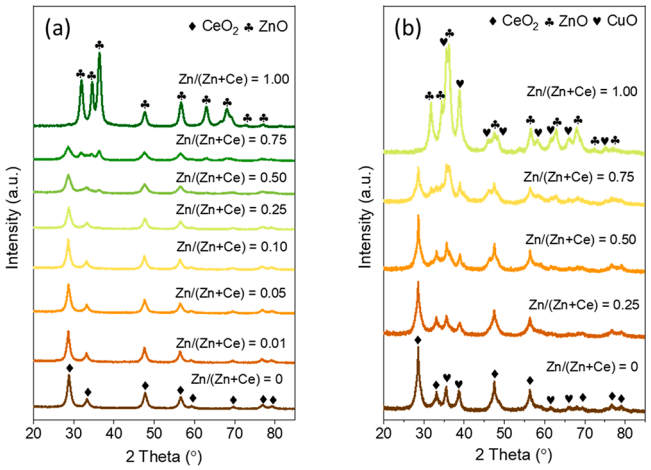

Figure 2. XRD patterns of (a) $Cu(5)/ZnO-CeO_2(y)$ and (b) $Cu(45)/ZnO-CeO_2(y)$ catalysts.

members of this series of catalysts exhibited XRD patterns coresponding to the fluorite and wurtzite structures of CeO_2 (PDF No. 00-004-0593) and ZnO (PDF No. 00-065-3411), respectively. The broadening of the diffraction peaks points to the nanocrystalline nature of the support material (CeO_2 or ZnO). All of the Ce-containing samples display clear diffraction peaks due to CeO_2. Zn addition led to a small shift of the CeO_2 (111) diffraction peaks to lower angle compared to $Cu(5)/CeO_2$ (Figure S2), pointing to the expansion of the CeO_2 lattice. As substitution of Ce^{4+} (0.97 Å) by the smaller Zn^{2+} (0.90 Å) would lead to a lattice contraction,[46] the observation of the opposite can be explained by the formation of reduced Ce sites. This does not exclude that a small part of copper is also included in CeO_2. Such substitution does not necessarily lead to a lattice parameter shift.[47] Only for catalysts with a high Zn content, *i.e.*, $y \geq 0.50$, clear ZnO diffraction peaks can be observed. No diffraction peaks assignable to CuO (PDF No. 00-041-0254) or Cu_2O (PDF No. 00-05-0667) are present in all the XRD patterns, indicating that the Cu phases in these catalysys are either well-dispersed or amorphous. The diffraction patterns of the Cu−Zn−Ce oxide catalysts with high Cu loading are shown in Figure 2b. Similar to the series of $Cu(5)/ZnO-CeO_2(y)$, CeO_2 diffraction peaks are present in all the Ce-containing samples and ZnO diffraction peaks are only observed in the samples with high Zn content ($y \geq 0.50$). Further, all the $Cu(45)/ZnO-CeO_2(y)$ catalysts display clear CuO diffraction peaks, which is expected given high Cu loading of these samples. Notably, the intensity of the CuO diffraction peaks are much weaker in the Ce-containing samples as compared to the Cu(45)/ZnO, indicating that the presence of CeO_2 can enhance Cu dispersion.

H_2-TPR was carried out to probe Cu-support interactions in the Cu−Zn−Ce oxide catalysts. Figure 3a shows that two distinct reduction peaks were observed in all the Ce-containing samples for the series of $Cu(5)/ZnO-CeO_2(y)$. These two reduction peaks (α and β) can be assigned, respectively, to dispersed Cu species strongly interacting with ceria support

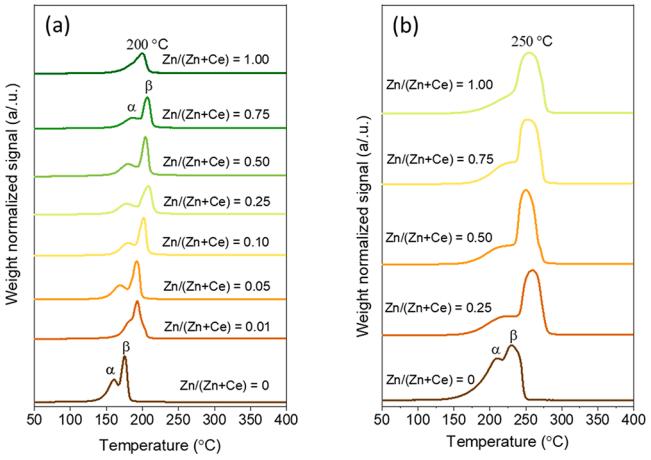

Figure 3. H_2-TPR profiles of (a) $Cu(5)/ZnO-CeO_2(y)$ and (b) $Cu(45)/ZnO-CeO_2(y)$ catalysts.

and a $Cu-CeO_2$ solid solution.[48,49] The amount of H_2 consumed was normalized to the Cu content (Table 1). As the resulting values were higher than unity (corresponding to the reduction of CuO to Cu), we can conclude that the ceria support was also reducing, implying the formation of oxygen vacancies. Moreover, similar two-peak reduction profiles were observed for all of the Ce-containing samples, implying that Cu preferably interacts with CeO_2 over ZnO in the ternary catalysts. It is also found that the α and β reduction peaks already shifted to higher temperatures after addition of a small amount of ZnO, which is likely related to the modification of CeO_2 support (as indicated by the XRD data) or the decoration of Cu particles by Zn species. The H_2-TPR profile of Cu(5)/ZnO sample shows an asymmetric reduction peak around 200 °C with a small low-temperature shoulder, which can be attributed to dispersed Cu species interacting with ZnO.[50] The Cu−Zn−Ce oxide catalysts with high Cu loading ($x = 45$) were also investigated by H_2-TPR. Figure 3b shows that the α and β reduction peaks in the Ce-containing samples and the main reduction peak in the Cu(45)/ZnO sample shifted to higher temperature in comparison to the catalysts with the same support composition in Figure 3a. Such shifts can be explained by the fact that Cu particles are much larger at higher Cu loading (see below).

We used N_2O titration to quantify the metallic Cu surface sites in the reduced Cu−Zn−Ce oxide catalysts, which is a key descriptor for methanol synthesis for Cu-based catalysts.[51,52] The results are listed in Table 1. The Cu dispersion as a function of Zn content in the support is also plotted in Figure 4. For the series of $Cu(5)/ZnO-CeO_2(y)$, Figure 4a shows that the Cu dispersion gradually decreases from ~60% for $Cu(5)/CeO_2$ to ~10% for Cu(5)/ZnO. The decreasing trend of Cu dispersion with respect to Zn content indicates that CeO_2 interacts stronger with Cu than ZnO.[20,53] Notably, the metallic Cu surface areas remain almost the same (~19 m^2/g_{cat}) after addition of a small amount of Zn ($y \leq 0.05$). In addition to metallic Cu sites, the N_2O titration data reveal that oxygen vacancies exist in the Ce-containing samples after H_2 reduction (Table 1). These findings agree with the quantitative H_2-TPR quantification analysis. The Cu dispersion data of the $Cu(45)/ZnO-CeO_2(y)$ series are plotted in Figure 4b. Clearly, the higher Cu loading in these catalysts leads to a much lower Cu dispersion. It is also shown that (i) all of the Ce-containing catalysts display similar Cu dispersion and (ii)

https://doi.org/10.1021/acscatal.1c00131
ACS Catal. 2021, 11, 4880−4892

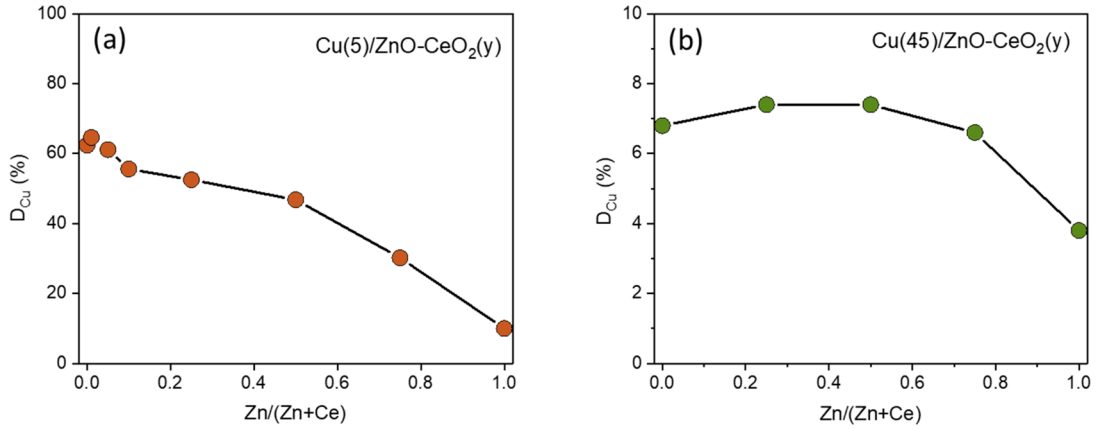

Figure 4. Cu dispersion of (a) Cu(5)/ZnO−CeO_2(y) and (b) Cu(45)/ZnO−CeO_2(y) catalysts determined from N_2O titration.

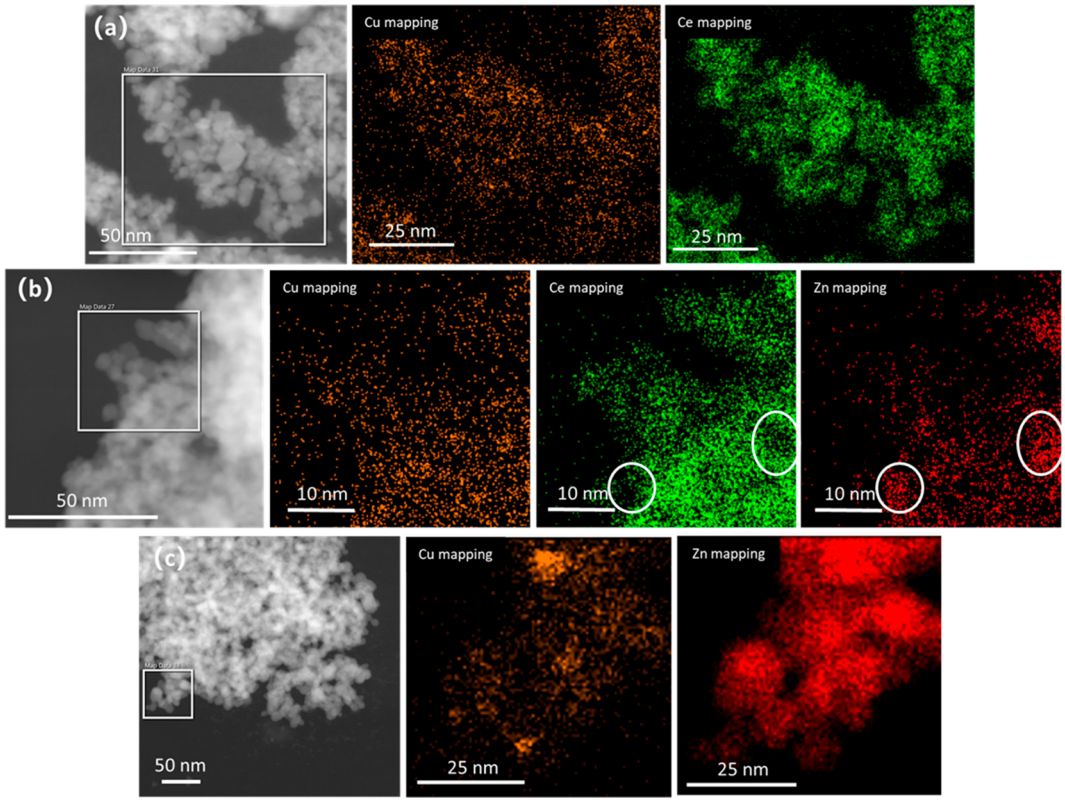

Figure 5. STEM images with corresponding elemental mappings of the reduced (a) Cu(5)/CeO_2, (b) Cu(5)/ZnO−CeO_2(0.25), and (c) Cu(5)/ZnO. Reduction conditions: 250 °C, 1 h, and 10 vol % H_2 in He.

the Cu(45)/ZnO exhibits the lowest Cu dispersion (3.8%) in this series.

STEM-EDX was used to investigate the elemental distribution (Cu, Zn and Ce) in the reduced Cu−Zn−Ce oxide catalysts (Figure 5). Although these data do not warrant a statistical analysis of the distribution of Zn and Ce in the support, inspection of the STEM-EDX mapping results points to the segregation of these two components at the nanometer scale (Figure 5b). Moreover, Cu is homogeneously and finely dispersed in the reduced Cu(5)/CeO_2 and Cu(5)/ZnO−CeO_2(0.25). In contrast, larger Cu particles can be distinguished in the reduced Cu(5)/ZnO. Clearly, the presence of CeO_2 in the support can increase Cu dispersion, in line with the N_2O titration results. To summarize, we demonstrate that FSP is a suitable method to prepare catalysts containing dispersed Cu particles supported on (mixed) oxides of CeO_2 and ZnO. The resulting catalysts display similar morphological and textural properties in a broad support compositional range. The Cu dispersion of FSP-prepared Cu−Zn−Ce oxide catalysts can be easily tuned by changing the Cu content and the Zn−Ce ratio in the precursor solutions.

3.2. Catalytic Activity Measurements. The series of Cu(5)/ZnO−CeO_2(y) catalysts were evaluated for CO_2 hydrogenation under the conditions of 250 °C and 30 bar. Figure 6a shows how CO_2 conversion and CH_3OH selectivity change with Zn content in the catalyst support. The CO_2 conversion is lowest for the Cu(5)/CeO_2 and increases with Zn content until y = 0.05. At higher Zn content ($0.05 \leq y \leq 0.75$), the ternary Cu−Zn−Ce oxide catalysts display nearly the same CO_2 conversion, while the Cu(5)/ZnO shows the

https://doi.org/10.1021/acscatal.1c00131
ACS Catal. 2021, 11, 4880−4892

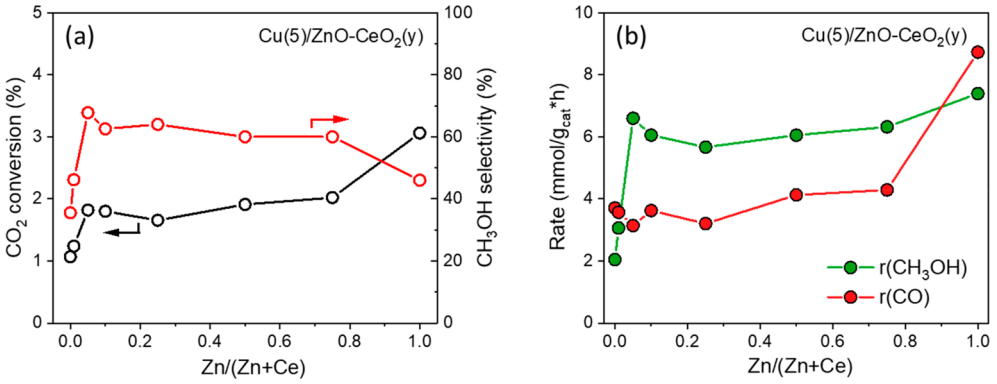

Figure 6. (a) CO_2 conversion and CH_3OH selectivity; (b) CH_3OH and CO formation rates as a function of support composition for Cu(5)/ZnO−CeO_2(y) catalysts. Reaction conditions: 250 °C, 30 bar, $H_2/CO_2/N_2$ = 3:1:1, and SV = 60 L/(g_{cat} × h).

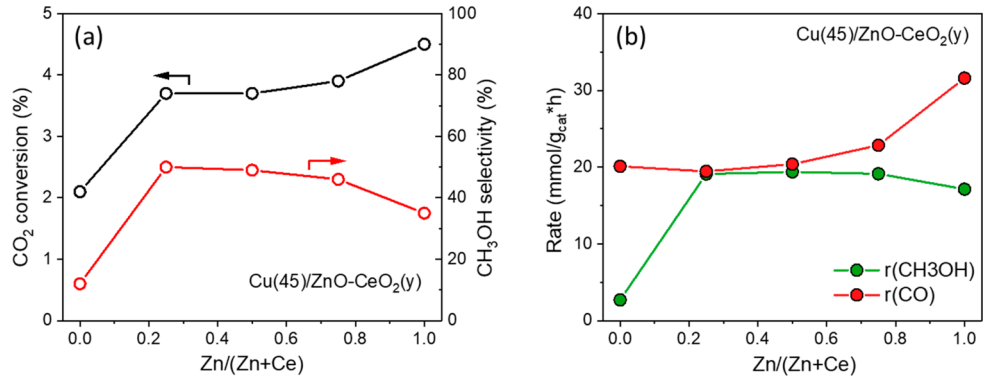

Figure 7. (a) CO_2 conversion and CH_3OH selectivity; (b) CH_3OH and CO formation rates as a function of support composition for Cu(45)/ZnO−CeO_2(y) catalysts. Reaction conditions: 250 °C, 30 bar, $H_2/CO_2/N_2$ = 3:1:1, and SV = 120 L/(g_{cat} × h).

highest CO_2 conversion. Regarding product distribution, we observe that the ternary Cu−Ze−Ce oxide catalysts show a higher CH_3OH selectivity compared to the binary Cu−Zn and Cu−Ce oxide catalysts. Figure 6b reports how CH_3OH and CO formation rates vary as a function of Zn content in the catalyst support. The CH_3OH formation rate increases more than twice after adding a small amount of ZnO ($y \leq 0.05$). As the Cu dispersion is nearly the same for these catalysts, the improved CH_3OH formation rate points to a clear Zn promotion effect on Cu surface for CH_3OH synthesis from CO_2.[54] At higher Zn content, the CH_3OH formation rate remains nearly unchanged, suggesting that a maximum Zn promotion is already achieved at a relatively low Zn content (y = 0.05). Regarding the formation of CO, the activity is similar for all the Ce-containing catalysts, while the corresponding rate of the Cu(5)/ZnO is nearly two times higher. These observations indicate that CeO_2 in these ternary catalysts can inhibit the rWGS reaction. As it has been suggested that CO can be a reaction intermediate for CH_3OH synthesis from CO_2 hydrogenation,[55] we also evaluated the activity of the Cu(5)/ZnO−CeO_2(y) catalysts in CO hydrogenation under the same conditions (Figure S4). The results show that the CH_3OH activity in CO hydrogenation decreased after adding a small amount of ZnO ($y \leq 0.05$) and remained nearly the same at higher ZnO content ($0.10 \leq y \leq 0.75$). Notably, all the Ce-containing catalysts displayed a significantly higher CH_3OH formation rate than Cu(5)/ZnO.

The Cu−Zn−Ce oxide catalysts with higher Cu loading (x = 45) were also tested in CO_2 hydrogenation. Similar trends of CO_2 conversion, CH_3OH selectivity and product formation rates as a function of Zn content were observed for this series of catalysts, irrespective of the substantial difference in Cu loading compared to Cu(5)/ZnO−CeO_2(y). Specifically, Figure 7a shows that (i) the Cu(45)/CeO_2 and Cu(45)/ZnO, respectively, have the lowest and highest CO_2 conversion and (ii) the ternary Cu−Zn−Ce oxide catalysts (y = 0.25, 0.50 and 0.75) have similar CO_2 conversion and higher CH_3OH selectivity than the corresponding binary catalysts. Figure 7b shows that addition of a small amount of ZnO (y = 0.25) leads to a significant increase in CH_3OH activity and a further increase in Zn content has a minor influence on CH_3OH activity. Addition of a large amount of ZnO (y = 0.75 and 1.00) resulted in a significant increase of CO activity. Besides these similarities, it was observed that the maximum Zn promotion for CH_3OH formation in Cu(45)/ZnO−CeO_2(y) catalysts (2.7 → 19.1 mmol/(g_{cat} × h)) is significantly higher than that in Cu(5)/ZnO−CeO_2(y) catalysts (2.0 → 6.6 mmol/(g_{cat} × h)). This difference implies that the Zn promotion for CH_3OH synthesis from CO_2 is dependent on Cu particle size.

We then compared the performance of a selected Cu−Zn−Ce oxide catalyst, *i.e.*, Cu(45)/ZnO−CeO_2(0.25) to a commercial MSC in CO_2 hydrogenation to CH_3OH. Figure 8 shows that the Cu−Zn−Ce oxide catalyst displays a higher initial CH_3OH selectivity than the commercial MSC at similar CO_2 conversion (~6%). Upon increasing time on stream (TOS), the CH_3OH selectivity of the Cu−Zn−Ce oxide catalyst slowly increased at the expense of CO_2 conversion. A similar trade-off between CH_3OH selectivity and CO_2 conversion has been earlier reported for Cu-based catalysts

https://doi.org/10.1021/acscatal.1c00131
ACS Catal. 2021, 11, 4880−4892

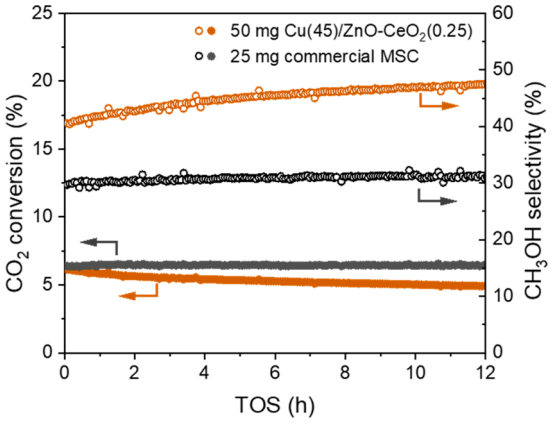

Figure 8. Time-on-stream CO_2 conversion and CH_3OH selectivity comparison between Cu(45)/ZnO−CeO_2(0.25) and commercial methanol synthesis catalysts. Reaction conditions: 250 °C, 30 bar, $H_2/CO_2/N_2$ = 30:10:10 (mL/min).

and can be attributed either to product inhibition by H_2O and/or CH_3OH or to CH_3OH decomposition.[56,57] After 12 h on stream, the CH_3OH selectivity of the Cu−Zn−Ce oxide catalyst was ∼16% higher than the commercial MSC. A catalyst stability test of 100 h (Figure S8) shows that the deactivation of Cu(45)/ZnO−CeO_2(0.25) was faster in the beginning (first 30 h) than after prolonged reaction. Notably, the CO formation rate decreased more substantially with time on stream than the CH_3OH formation rate.

3.3. In Situ IR Spectroscopy. CO adsorption was carried out to characterize the Cu speciation in the reduced Cu−Zn−Ce oxide catalysts. For the Cu/CeO_2 sample, we observed that the carbonyl band at 2068 cm^{-1} strongly blue-shifted with increasing CO partial pressure (Figure 9a). The shift is due to dipole−dipole coupling of CO molecules adsorbed on metallic Cu sites.[58] The presence of a weak broad band around 1960 cm^{-1} due to bridge-bound carbonyls on metallic Cu confirms this assignment. The low-frequency tailing of the band can be explained by the presence of a range of Cu particle sizes with different extents of dipole−dipole coupling interactions. The spectra also feature a strong band at 2109 cm^{-1}, which can be assigned to interfacial Cu^+ sites as reported before for reduced Cu/CeO_2.[59−61] The corresponding CO IR spectra of Cu/ZnO in Figure 9b show a much lower intensity of carbonyl bands, which is in keeping with the lower Cu dispersion. Similar spectra have been reported in literature for Cu/ZnO.[62−64] The most likely interpretation is that the 2087 cm^{-1} band is due to carbonyl on metallic Cu and the broad band at lower frequency to Zn-decorated Cu sites.[65] The CO IR spectra of Cu(5)/ZnO−CeO_2(0.05) resemble the one of Cu/ZnO with a substantially higher intensity (Figure 9c). Accordingly, we assign these spectra to similar Zn-decorated Cu sites as in Cu/ZnO but with a much higher dispersion. Notably, the carbonyl band due to Cu^+ sites is absent in the reduced ternary catalyst. Although this may indicate that the Cu−CeO_2 interface is lost, we tentatively assign the difference with Cu/CeO_2 to Zn decoration of the Cu surface.

We also investigated the surface of the reduced Cu−Zn−Ce oxide catalysts by IR spectroscopy during temperature-programmed CO_2 hydrogenation. The C−H vibration and carbonyl regions are displayed in Figure 10. For all of the catalysts, formate was present on the Cu surface (HCOO-Cu) with increasing temperature to 250 °C as evidenced by the band at 2849 cm^{-1}.[52,66−68] The band at 2876 cm^{-1} in the C−H vibration region observed for Cu/ZnO can be attributed to formate adsorbed on ZnO (HCOO-Zn).[68,69] Notably, formates were formed at lower temperature on Cu/ZnO compared to the other two catalysts. A comparison of Cu(5)/ZnO−CeO_2(0.05) and Cu(5)/CeO_2 shows that ZnO addition led to a carbonyl band at 2120 cm^{-1} in the spectrum at 50 °C. The Cu/ZnO sample also contains a weaker carbonyl band at 2104 cm^{-1}. This carbonyl band is less stable on Cu/ZnO than on Cu(5)/ZnO−CeO_2(0.05) as can be appreciated by comparison of spectra with increasing temperature (Figure 10b,c). Clearly, the appearance of carbonyl bands for the two Zn-containing catalysts points to facile CO_2 activation on Zn-decorated Cu. Furthermore, the carbonyl bands observed during CO_2 hydrogenation at 50 °C were substantially blue-shifted in comparison to those recorded upon CO adsorption (Figure 9). We also observed that the carbonyl band on Cu(5)/ZnO−CeO_2(0.05) was located at a higher wavenumber (2120 cm^{-1}) than on Cu/ZnO (2104 cm^{-1}). Such difference can be explained by electron depletion of the Cu surface, which may be due to the high coverage of oxygen caused by CO_2 dissociation at this temperature. A similar effect was also observed by comparing the spectra recorded at 250 °C where formate is the electro-withdrawing adsorbate.[70−72] It was found that the intensity of the HCOO-Cu band on Cu(5)/

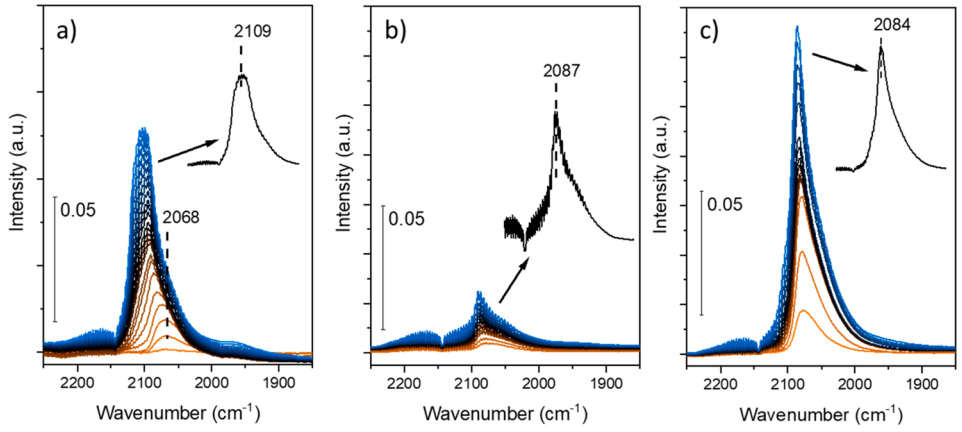

Figure 9. IR spectra of CO adsorbed on reduced (a) Cu(5)/CeO_2, (b) Cu(5)/ZnO, and (c) Cu(5)/ZnO−CeO_2(0.05) (T_{ads} = 40 °C with increasing CO partial pressure from orange to blue with a maximum CO partial pressure of 10 mbar).

https://doi.org/10.1021/acscatal.1c00131
ACS Catal. 2021, 11, 4880−4892

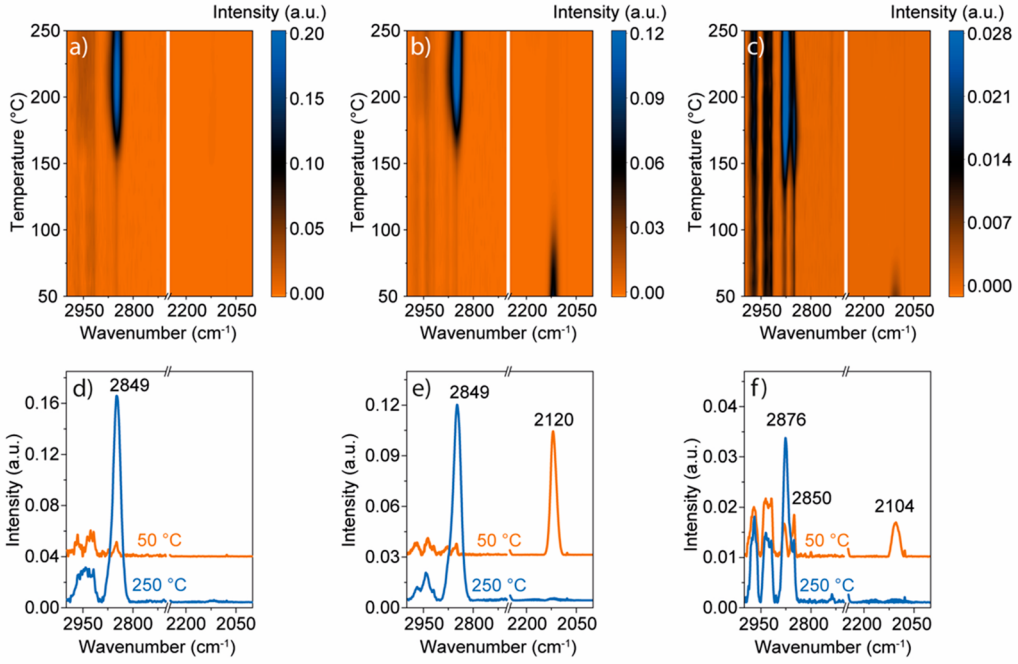

Figure 10. IR spectra during CO_2 hydrogenation over (a) Cu(5)/CeO_2, (b) Cu(5)/ZnO−CeO_2(0.05), and (c) Cu(5)/ZnO. IR spectra at reaction temperature of 50 and 250 °C over (d) Cu(5)/CeO_2, (e) Cu(5)/ZnO−CeO_2(0.05), and (f) Cu(5)/ZnO. Reaction conditions: CO_2 5%, H_2 15%, He 80%, total flow of 200 mL/min, and 50−250 °C.

CeO_2 and Cu(5)/ZnO−CeO_2(0.05) were much higher than on Cu(5)/ZnO, indicating a higher formate coverage on the Ce-containing catalysts.

3.4. Discussion. A key finding from the results of this work is that the combination of Cu with ZnO−CeO_2 supports results in a higher CH_3OH selectivity in CO_2 hydrogenation in comparison with binary Cu/ZnO and Cu/CeO_2 catalysts. The role of CeO_2 oxygen vacancies in CO_2 conversion was examined because such vacancies are known to play an important role in many ceria-based catalysts.[73,74] For this purpose, we plotted CH_3OH and CO formation rates against the amount of oxygen vacancy estimated by H_2-TPR and N_2O titration measurements (Figure S9). The absence of strong correlations indicates that oxygen vacancies in CeO_2 support are not the key descriptor for CO_2 hydrogenation to CH_3OH or CO. The blocking of oxygen vacancies by in situ formed carbonates may explain their limited role in CO_2 hydrogenation.[21,45,75]

We next discuss the improved CH_3OH selectivity in the context of Cu−ZnO and Cu−CeO_2 interactions. Scheme 1 presents three simplified models for the Cu/CeO_2, Cu/ZnO−CeO_2, and Cu/ZnO catalysts investigated in this work. To facilitate the discussion, turnover frequencies (TOFs) for CH_3OH and CO formation are plotted against the Cu particle sizes estimated by N_2O titration (Figure S10). On the one hand, the improved CH_3OH selectivity is clearly related to Zn addition to Cu/CeO_2, which promotes CH_3OH reaction rate as shown in the catalytic data. We found that such Zn promotion already reaches its full extent at a relatively low Zn content, e.g., in Cu(5)/ZnO−CeO_2(0.05). As diffraction peaks due to bulk ZnO are absent in the XRD pattern of this catalyst, the Zn promotion of CH_3OH synthesis can be correlated to highly dispersed Zn species on Cu as also suggested in an earlier study.[76] A comparison of CO IR spectra (Figure 9) shows that the ternary catalysts are not a physical mixture of Cu/CeO_2 and Cu/ZnO. The addition of ZnO to Cu/CeO_2 results in the formation of Zn-decorated Cu sites upon reduction of Cu(5)/ZnO−CeO_2(0.05) as also observed for Cu(5)/ZnO. The formation of Zn-decorated metallic Cu in Cu/ZnO as active sites for CH_3OH synthesis has been well documented,[2,54,77] with main propositions for the formation of ZnO_x moieties on Cu surface and a CuZn surface alloy. Comparing the CO IR spectra of our catalysts to those reported for Cu/ZnO by Topsoe et al.,[62,64] it is more likely that Cu is modified by ZnO_x in our catalysts. This is consistent with the relatively low reduction temperature employed. On the other hand, CeO_2 addition inhibits the rWGS reaction as can be inferred from Figure S10b: all the Ce-containing catalysts display significantly lower TOF(CO) compared to Cu/ZnO. In situ IR spectra recorded at 250 °C during CO_2 hydrogenation indicate that the formate coverage on Cu is higher on Ce-containing catalysts than on Cu/ZnO. We propose that the ceria-induced inhibition of the rWGS is associated with the higher formate coverage, which blocks metallic Cu sites active in the rWGS as proposed

Scheme 1. Proposed Models of FSP-Prepared Cu/CeO_2, Cu/ZnO−CeO_2, and Cu/ZnO Catalysts

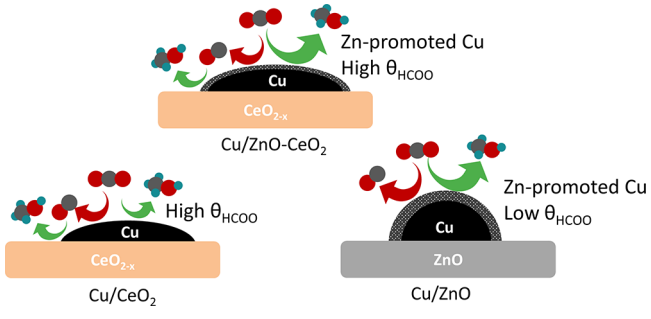

https://doi.org/10.1021/acscatal.1c00131
ACS Catal. 2021, 11, 4880−4892

before.[45,78−81] Besides the blocking of Cu surface by formate, in situ CO-to-CH_3OH conversion during CO_2 hydrogenation can also contribute to the ceria-induced inhibition of the rWGS. It has been reported that Cu−CeO_2 interface is highly active for CO hydrogenation to CH_3OH.[21,22] Our catalytic data (Figure S4) also show that the Ce-containing catalysts showed a substantially higher CH_3OH formation rate in CO hydrogenation than Cu/ZnO catalyst. As such, we propose that the ceria-induced rWGS inhibition can also be due to the fact that the in situ formed CO during CO_2 hydrogenation can be faster hydrogenated to CH_3OH at Cu−CeO_2 interface in Ce-containing catalysts than Cu/ZnO.

4. CONCLUSIONS

Well-defined high-surface-area Cu−Zn−Ce oxide catalysts were prepared by a one-step FSP method. The Cu loading and support composition were systematically varied to investigate how Cu-support interactions affect CO_2 hydrogenation. CeO_2 interacts more strongly with Cu than ZnO, leading to a better Cu dispersion in the presence of CeO_2. CO_2 hydrogenation results show that (i) the Cu−Zn−Ce oxide catalysts display a significantly higher CH_3OH selectivity in comparison to the binary Cu−Zn and Cu−Ce catalysts and (ii) the Cu−Zn−Ce oxide catalyst with a high Cu loading (∼40 wt %) outperforms a commercial methanol synthesis catalyst in terms of CH_3OH selectivity. Evaluation of the relation between the structure and the catalytic performance reveals that the improved CH_3OH selectivity of Cu−Zn−Ce oxide catalysts can be explained by Zn promotion of the Cu surface for CO_2 hydrogenation to CH_3OH and by ceria-induced inhibition of the rWGS reaction. Based on in situ IR studies and other characterization results, we propose that (i) the promotion of CH_3OH synthesis from CO_2 is due to the formation of Zn-decorated Cu sites and (ii) the ceria-induced inhibition of the rWGS can be explained by blocking of the Cu surface by formate species and a higher rate of hydrogenation of the CO intermediate. This study also demonstrates that FSP is a promising method to prepare multicomponent methanol synthesis catalysts. The use of different metal oxide promoters that affect Cu-support interactions can help to improve the overall performance of methanol synthesis catalysts in CO_2 hydrogenation.

■ ASSOCIATED CONTENT

Supporting Information

The Supporting Information is available free of charge at https://pubs.acs.org/doi/10.1021/acscatal.1c00131.

Additional characterization (TEM, XRD, and H_2-TPR) and catalytic test results (CO vs CO_2 hydrogenation) of the Cu−Zn−Ce oxide and commercial methanol synthesis catalysts (Figures S1−S4); experimental results of the Cu−Zn−Ce oxide catalysts with an intermediate Cu loading (Table S1 and Figures S5−S7); catalyst stability test of Cu(45)/ZnO−CeO_2(0.25) in CO_2 hydrogenation (Figure S8); correlations between CH_3OH and CO formation rates and the amount of oxygen vacancies (Figure S9); correlations between turnover frequencies (CH_3OH and CO) and estimated Cu particle size (Figure S10) (PDF)

■ AUTHOR INFORMATION

Corresponding Author

Emiel J. M. Hensen − *Laboratory of Inorganic Materials and Catalysis, Department of Chemical Engineering and Chemistry, Eindhoven University of Technology, 5600 MB Eindhoven, The Netherlands;* orcid.org/0000-0002-9754-2417; Email: e.j.m.hensen@tue.nl

Authors

Jiadong Zhu − *Laboratory of Inorganic Materials and Catalysis, Department of Chemical Engineering and Chemistry, Eindhoven University of Technology, 5600 MB Eindhoven, The Netherlands*

Diana Ciolca − *Laboratory of Inorganic Materials and Catalysis, Department of Chemical Engineering and Chemistry, Eindhoven University of Technology, 5600 MB Eindhoven, The Netherlands*

Liang Liu − *Laboratory of Inorganic Materials and Catalysis, Department of Chemical Engineering and Chemistry, Eindhoven University of Technology, 5600 MB Eindhoven, The Netherlands*

Alexander Parastaev − *Laboratory of Inorganic Materials and Catalysis, Department of Chemical Engineering and Chemistry, Eindhoven University of Technology, 5600 MB Eindhoven, The Netherlands*

Nikolay Kosinov − *Laboratory of Inorganic Materials and Catalysis, Department of Chemical Engineering and Chemistry, Eindhoven University of Technology, 5600 MB Eindhoven, The Netherlands;* orcid.org/0000-0001-8520-4886

Complete contact information is available at: https://pubs.acs.org/10.1021/acscatal.1c00131

Notes

The authors declare no competing financial interest.

■ ACKNOWLEDGMENTS

The authors acknowledge financial support from The Netherlands Organization for Scientific Research (NWO) for a Vici grant. Mengyue Wu (TU Delft) is acknowledged for carrying out the STEM-EDX measurements and Adelheid Elemans-Mehring (TU Eindhoven) for performing elemental analysis.

■ REFERENCES

(1) Sehested, J. Industrial and Scientific Directions of Methanol Catalyst Development. *J. Catal.* **2019**, *371*, 368−375.

(2) Behrens, M.; Studt, F.; Kasatkin, I.; Kühl, S.; Hävecker, M.; Abild-pedersen, F.; Zander, S.; Girgsdies, F.; Kurr, P.; Kniep, B.; Tovar, M.; Fischer, R. W.; Nørskov, J. K.; Schlögl, R. The Active Site of Methanol Synthesis over Cu/ZnO/Al2O3 Industrial Catalysts. *Science* **2012**, *336*, 893−898.

(3) Zhong, J.; Yang, X.; Wu, Z.; Liang, B.; Huang, Y.; Zhang, T. State of the Art and Perspectives in Heterogeneous Catalysis of CO2 Hydrogenation to Methanol. *Chem. Soc. Rev.* **2020**, *49*, 1385−1413.

(4) Goeppert, A.; Czaun, M.; Jones, J.-P.; Surya Prakash, G. K.; Olah, G. A. Recycling of Carbon Dioxide to Methanol and Derived Products − Closing the Loop. *Chem. Soc. Rev.* **2014**, *43*, 7995−8048.

(5) Olah, G. A. Beyond Oil and Gas: The Methanol Economy. *Angew. Chem., Int. Ed.* **2005**, *44*, 2636−2639.

(6) Chinchen, G. C.; Denny, P. J.; Parker, D. G.; Spencer, M. S.; Whan, D. A. Mechanism of Methanol Synthesis from CO2/CO/H2Mixtures over Copper/Zinc Oxide/Alumina Catalysts: Use of 14C-Labelled Reactants. *Appl. Catal.* **1987**, *30*, 333−338.

(7) Xu, D.; Wu, P.; Yang, B. Origin of CO2 as the Main Carbon Source in Syngas-to-Methanol Process over Cu: Theoretical Evidence from a Combined DFT and Microkinetic Modeling Study. *Catal. Sci. Technol.* **2020**, *10*, 3346−3352.
(8) Behrens, M. Promoting the Synthesis of Methanol: Understanding the Requirements for an Industrial Catalyst for the Conversion of CO2. *Angew. Chem., Int. Ed.* **2016**, *55*, 14906−14908.
(9) Prašnikar, A.; Pavlišič, A.; Ruiz-Zepeda, F.; Kovač, J.; Likozar, B. Mechanisms of Copper-Based Catalyst Deactivation during CO2 Reduction to Methanol. *Ind. Eng. Chem. Res.* **2019**, *58*, 13021−13029.
(10) Liang, B.; Ma, J.; Su, X.; Yang, C.; Duan, H.; Zhou, H.; Deng, S.; Li, L.; Huang, Y. Investigation on Deactivation of Cu/ZnO/Al2O3 Catalyst for CO2 Hydrogenation to Methanol. *Ind. Eng. Chem. Res.* **2019**, *58*, 9030−9037.
(11) Lunkenbein, T.; Girgsdies, F.; Kandemir, T.; Thomas, N.; Behrens, M.; Schlögl, R.; Frei, E. Bridging the Time Gap: A Copper/Zinc Oxide/Aluminum Oxide Catalyst for Methanol Synthesis Studied under Industrially Relevant Conditions and Time Scales. *Angew. Chem., Int. Ed.* **2016**, *55*, 12708−12712.
(12) Wu, J.; Saito, M.; Takeuchi, M.; Watanabe, T. The Stability of Cu/ZnO-Based Catalysts in Methanol Synthesis from a CO2-Rich Feed and from a CO-Rich Feed. *Appl. Catal., A* **2001**, *218*, 235−240.
(13) Wang, Y.; Kattel, S.; Gao, W.; Li, K.; Liu, P.; Chen, J. G.; Wang, H. Exploring the Ternary Interactions in Cu−ZnO−ZrO2 Catalysts for Efficient CO2 Hydrogenation to Methanol. *Nat. Commun.* **2019**, *10*, 1166−1175.
(14) Arena, F.; Italiano, G.; Barbera, K.; Bordiga, S.; Bonura, G.; Spadaro, L.; Frusteri, F. Solid-State Interactions, Adsorption Sites and Functionality of Cu−ZnO/ZrO2 Catalysts in the CO2 Hydrogenation to CH3OH. *Appl. Catal., A* **2008**, *350*, 16−23.
(15) Arena, F.; Barbera, K.; Italiano, G.; Bonura, G.; Spadaro, L.; Frusteri, F. Synthesis, Characterization and Activity Pattern of Cu−ZnO/ZrO2 Catalysts in the Hydrogenation of Carbon Dioxide to Methanol. *J. Catal.* **2007**, *249*, 185−194.
(16) Guo, X.; Mao, D.; Lu, G.; Wang, S.; Wu, G. Glycine-Nitrate Combustion Synthesis of CuO-ZnO-ZrO2 Catalysts for Methanol Synthesis from CO2 Hydrogenation. *J. Catal.* **2010**, *271*, 178−185.
(17) Chang, K.; Zhang, H.; Cheng, M.; Lu, Q. Application of Ceria in CO2 Conversion Catalysis. *ACS Catal.* **2020**, *10*, 613−631.
(18) Hu, X.; Qin, W.; Guan, Q.; Li, W. The Synergistic Effect of CuZnCeOx in Controlling the Formation of Methanol and CO from CO2 Hydrogenation. *ChemCatChem* **2018**, *10*, 4438−4449.
(19) Zhao, B.; Pan, Y. X.; Liu, C. J. The Promotion Effect of CeO2 on CO2 Adsorption and Hydrogenation over Ga2O3. *Catal. Today* **2012**, *194*, 60−64.
(20) Konsolakis, M. The Role of Copper−Ceria Interactions in Catalysis Science: Recent Theoretical and Experimental Advances. *Appl. Catal., B* **2016**, *198*, 49−66.
(21) van de Water, L. G. A.; Wilkinson, S. K.; Smith, R. A. P.; Watson, M. J. Understanding Methanol Synthesis from CO/H2 Feeds over Cu/CeO2 Catalysts. *J. Catal.* **2018**, *364*, 57−68.
(22) Shen, W.-J.; Ichihashi, Y.; Matsumura, Y. Low Temperature Methanol Synthesis from Carbon Monoxide and Hydrogen over Ceria Supported Copper Catalyst. *Appl. Catal., A* **2005**, *282*, 221−226.
(23) Graciani, J.; Mudiyanselage, K.; Xu, F.; Baber, A. E.; Evans, J.; Senanayake, S. D.; Stacchiola, D. J.; Liu, P.; Hrbek, J.; Sanz, J. F.; Rodriguez, J. A. Highly Active Copper-Ceria and Copper-Ceria-Titania Catalysts for Methanol Synthesis from CO2. *Science* **2014**, *345*, 546−550.
(24) Bonura, G.; Arena, F.; Mezzatesta, G.; Cannilla, C.; Spadaro, L.; Frusteri, F. Role of the Ceria Promoter and Carrier on the Functionality of Cu-Based Catalysts in the CO2-to-Methanol Hydrogenation Reaction. *Catal. Today* **2011**, *171*, 251−256.
(25) Gao, P.; Li, F.; Zhao, N.; Xiao, F.; Wei, W.; Zhong, L.; Sun, Y. Influence of Modifier (Mn, La, Ce, Zr and Y) on the Performance of Cu/Zn/Al Catalysts via Hydrotalcite-like Precursors for CO2 Hydrogenation to Methanol. *Appl. Catal., A* **2013**, *468*, 442−452.
(26) Arena, F.; Mezzatesta, G.; Zafarana, G.; Trunfio, G.; Frusteri, F.; Spadaro, L. How Oxide Carriers Control the Catalytic Functionality of the Cu−ZnO System in the Hydrogenation of CO2 to Methanol. *Catal. Today* **2013**, *210*, 39−46.
(27) Arena, F.; Mezzatesta, G.; Zafarana, G.; Trunfio, G.; Frusteri, F.; Spadaro, L. Effects of Oxide Carriers on Surface Functionality and Process Performance of the Cu−ZnO System in the Synthesis of Methanol via CO2 Hydrogenation. *J. Catal.* **2013**, *300*, 141−151.
(28) Chang, K.; Wang, T.; Chen, J. G. Methanol Synthesis from CO2 Hydrogenation over CuZnCeTi Mixed Oxide Catalysts. *Ind. Eng. Chem. Res.* **2019**, *58*, 7922−7928.
(29) Schumann, J.; Eichelbaum, M.; Lunkenbein, T.; Thomas, N.; Álvarez Galván, M. C.; Schlögl, R.; Behrens, M. Promoting Strong Metal Support Interaction: Doping ZnO for Enhanced Activity of Cu/ZnO:M (M = Al, Ga, Mg) Catalysts. *ACS Catal.* **2015**, *5*, 3260−3270.
(30) Lei, H.; Nie, R.; Wu, G.; Hou, Z. Hydrogenation of CO2 to CH3OH over Cu/ZnO Catalysts with Different ZnO Morphology. *Fuel* **2015**, *154*, 161−166.
(31) Perego, C.; Villa, P. Catalyst Preparation Methods. *Catal. Today* **1997**, *34*, 281−305.
(32) Wu, J.; Luo, S.; Toyir, J.; Saito, M.; Takeuchi, M.; Watanabe, T. Optimization of Preparation Conditions and Improvement of Stability of Cu/ZnO-Based Multicomponent Catalysts for Methanol Synthesis from CO2 and H2. *Catal. Today* **1998**, *45*, 215−220.
(33) Baltes, C.; Vukojevic, S.; Schuth, F. Correlations between Synthesis, Precursor, and Catalyst Structure and Activity of a Large Set of CuO/ZnO/Al2O3 Catalysts for Methanol Synthesis. *J. Catal.* **2008**, *258*, 334−344.
(34) Behrens, M. Meso- and Nano-Structuring of Industrial Cu/ZnO/(Al2O3) Catalysts. *J. Catal.* **2009**, *267*, 24−29.
(35) Schwarz, J. A.; Contescu, C.; Contescu, A. Methods for Preparation of Catalytic Materials. *Chem. Rev.* **1995**, *95*, 477−510.
(36) Tada, S.; Fujiwara, K.; Yamamura, T.; Nishijima, M.; Uchida, S.; Kikuchi, R. Flame Spray Pyrolysis Makes Highly Loaded Cu Nanoparticles on ZrO2 for CO2-to-Methanol Hydrogenation. *Chem. Eng. J.* **2020**, *381*, 122750−122760.
(37) Tada, S.; Larmier, K.; Büchel, R.; Copéret, C. Methanol Synthesis: Via CO2 Hydrogenation over CuO-ZrO2 Prepared by Two-Nozzle Flame Spray Pyrolysis. *Catal. Sci. Technol.* **2018**, *8*, 2056−2060.
(38) Ahmad, R.; Hellinger, M.; Buchholz, M.; Sezen, H.; Gharnati, L.; Wöll, C.; Sauer, J.; Döring, M.; Grunwaldt, J. D.; Arnold, U. Flame-Made Cu/ZnO/Al2O3 Catalyst for Dimethyl Ether Production. *Catal. Commun.* **2014**, *43*, 52−56.
(39) Wegner, K.; Schimmoller, B.; Thiebaut, B.; Fernandez, C.; Rao, T. N. Pilot Plants for Industrial Nanoparticle Production by Flame Spray Pyrolysis. *KONA* **2011**, *29*, 251−265.
(40) Huber, F.; Meland, H.; Rønning, M.; Venvik, H.; Holmen, A. Comparison of Cu-Ce-Zr and Cu-Zn-Al Mixed Oxide Catalysts for Water-Gas Shift. *Top. Catal.* **2007**, *45*, 101−104.
(41) Jensen, J. R.; Johannessen, T.; Wedel, S.; Livbjerg, H. A Study of Cu/ZnO/Al2O3Methanol Catalysts Prepared by Flame Combustion Synthesis. *J. Catal.* **2003**, *218*, 67−77.
(42) Koirala, R.; Pratsinis, S. E.; Baiker, A. Synthesis of Catalytic Materials in Flames: Opportunities and Challenges. *Chem. Soc. Rev.* **2016**, *45*, 3053−3068.
(43) Teoh, W. Y.; Amal, R.; Madler, L. Flame Spray Pyrolysis: An Enabling Technology for Nanoparticles Design and Fabrication. *Nanoscale* **2010**, *2*, 1324−1347.
(44) Takeguchi, T.; Manabe, S.; Kikuchi, R.; Eguchi, K.; Kanazawa, T.; Matsumoto, S.; Ueda, W. Determination of Dispersion of Precious Metals on CeO2- Containing Supports. *Appl. Catal., A* **2005**, *293*, 91−96.
(45) Zhu, J.; Su, Y.-Q.; Chai, J.; Muravev, V.; Kosinov, N. A.; Hensen, E. J. M. Mechanism and Nature of Active Sites for Methanol Synthesis from CO/CO2 on Cu/CeO2. *ACS Catal.* **2020**, *10*, 11532−11544.

https://doi.org/10.1021/acscatal.1c00131
ACS Catal. 2021, 11, 4880−4892

(46) Du, H.; Wang, Y.; Arandiyan, H.; Scott, J.; Wan, T.; Chu, D. Correlating Morphology and Doping Effects with the Carbon Monoxide Catalytic Activity of Zn Doped CeO2 Nanocrystals. *Catal. Sci. Technol.* **2018**, *8*, 134−138.
(47) Wang, X.; Rodriguez, J. A.; Hanson, J. C.; Gamarra, D.; Martínez-Arias, A.; Fernández-García, M. Unusual Physical and Chemical Properties of Cu in Ce 1-XCu XO 2 Oxides. *J. Phys. Chem. B* **2005**, *109*, 19595−19603.
(48) Wang, W. W.; Du, P. P.; Zou, S. H.; He, H. Y.; Wang, R. X.; Jin, Z.; Shi, S.; Huang, Y. Y.; Si, R.; Song, Q. S.; Jia, C. J.; Yan, C. H. Highly Dispersed Copper Oxide Clusters as Active Species in Copper-Ceria Catalyst for Preferential Oxidation of Carbon Monoxide. *ACS Catal.* **2015**, *5*, 2088−2099.
(49) Wang, W.-W.; Yu, W.-Z.; Du, P.-P.; Xu, H.; Jin, Z.; Si, R.; Ma, C.; Shi, S.; Jia, C.-J.; Yan, C.-H. Crystal Plane Effect of Ceria on Supported Copper Oxide Cluster Catalyst for CO Oxidation: Importance of Metal−Support Interaction. *ACS Catal.* **2017**, *7*, 1313−1329.
(50) Natesakhawat, S.; Lekse, J. W.; Baltrus, J. P.; Ohodnicki, P. R.; Howard, B. H.; Deng, X.; Matranga, C. Active Sites and Structure−Activity Relationships of Copper-Based Catalysts for Carbon Dioxide Hydrogenation to Methanol. *ACS Catal.* **2012**, *2*, 1667−1676.
(51) van den Berg, R.; Prieto, G.; Korpershoek, G.; van der Wal, L. I.; van Bunningen, A. J.; Lægsgaard-Jørgensen, S.; de Jongh, P. E.; de Jong, K. P. Structure Sensitivity of Cu and CuZn Catalysts Relevant to Industrial Methanol Synthesis. *Nat. Commun.* **2016**, *7*, 13057−13063.
(52) Karelovic, A.; Galdames, G.; Medina, J. C.; Yévenes, C.; Barra, Y. Mechanism and Structure Sensitivity of Methanol Synthesis from CO2 over SiO2 -Supported Cu Nanoparticles. *J. Catal.* **2019**, *369*, 415−426.
(53) Kydd, R.; Teoh, W. Y.; Wong, K.; Wang, Y.; Scott, J.; Zeng, Q. H.; Yu, A. B.; Zou, J.; Amal, R. Flame-Synthesized Ceria-Supported Copper Dimers for Preferential Oxidation of CO. *Adv. Funct. Mater.* **2009**, *19*, 369−377.
(54) Kuld, S.; Thorhauge, M.; Falsig, H.; Elkjær, C. F.; Helveg, S.; Chorkendorff, I.; Sehested, J. Quantifying the Promotion of Cu Catalysts by ZnO for Methanol Synthesis. *Science* **2016**, *352*, 969−974.
(55) Kattel, S.; Yan, B.; Yang, Y.; Chen, J. G.; Liu, P. Optimizing Binding Energies of Key Intermediates for CO2 Hydrogenation to Methanol over Oxide-Supported Copper. *J. Am. Chem. Soc.* **2016**, *138*, 12440−12450.
(56) Larmier, K.; Liao, W.-C.; Tada, S.; Lam, E.; Verel, R.; Bansode, A.; Urakawa, A.; Comas-Vives, A.; Copéret, C. CO2 -to-Methanol Hydrogenation on Zirconia-Supported Copper Nanoparticles: Reaction Intermediates and the Role of the Metal-Support. *Angew. Chem., Int. Ed.* **2017**, *56*, 2318−2323.
(57) Tada, S.; Watanabe, F.; Kiyota, K.; Shimoda, N.; Hayashi, R.; Takahashi, M.; Nariyuki, A.; Igarashi, A.; Satokawa, S. Ag Addition to CuO-ZrO2 Catalysts Promotes Methanol Synthesis via CO2 Hydrogenation. *J. Catal.* **2017**, *351*, 107−118.
(58) Browne, V. M.; Fox, S. G.; Hollins, P. Coupling Effects in Infrared Spectra from Supported Metal Catalyts. *Mater. Chem. Phys.* **1991**, *29*, 235−244.
(59) Martínez-Arias, A.; Fernández-García, M.; Soria, J.; Conesa, J. C. Spectroscopic Study of a Cu/CeO2 Catalyst Subjected to Redox Treatments in Carbon Monoxide and Oxygen. *J. Catal.* **1999**, *182*, 367−377.
(60) Bera, P.; Camara, A. L.; Hornes, A.; Martinez-Arias, A. Comparative in Situ DRIFTS-MS Study of 12CO- and 13CO-TPR on CuO/CeO2 Catalyst. *J. Phys. Chem. C* **2009**, *113*, 10689−10695.
(61) Chen, A.; Yu, X.; Zhou, Y.; Miao, S.; Li, Y.; Kuld, S.; Sehested, J.; Liu, J.; Aoki, T.; Hong, S.; Camellone, M. F.; Fabris, S.; Ning, J.; Jin, C.; Yang, C.; Nefedov, A.; Wöll, C.; Wang, Y.; Shen, J. Structure of the Catalytically Active Copper−Ceria Interfacial Perimeter. *Nat. Catal.* **2019**, *2*, 334−341.
(62) Topsøe, N. Y.; Topsøe, H. On the Nature of Surface Structural Changes in Cu/ZnO Methanol Synthesis Catalysts. *Top. Catal.* **1999**, *8*, 267−270.
(63) Naumann D'Alnoncourt, R.; Xia, X.; Strunk, J.; Löffler, E.; Hinrichsen, O.; Muhler, M. The Influence of Strongly Reducing Conditions on Strong Metal-Support Interactions in Cu/ZnO Catalysts Used for Methanol Synthesis. *Phys. Chem. Chem. Phys.* **2006**, *8*, 1525−1538.
(64) Topsøe, N. Y.; Topsøe, H. FTIR Studies of Dynamic Surface Structural Changes in Cu-Based Methanol Synthesis Catalysts. *J. Mol. Catal. A: Chem.* **1999**, *141*, 95−105.
(65) Greeley, J.; Gokhale, A. A.; Kreuser, J.; Dumesic, J. A.; Topsøe, H.; Topsøe, N. Y.; Mavrikakis, M. CO Vibrational Frequencies on Methanol Synthesis Catalysts: A DFT Study. *J. Catal.* **2003**, *213*, 63−72.
(66) Clarke, D. B.; Bell, A. T. An Infrared Study of Methanol Synthesis from CO2 on Clean and Potassium-Promoted Cu/SiO2. *J. Catal.* **1995**, *154*, 314−328.
(67) Bando, K. K.; Sayama, K.; Kusama, H.; Okabe, K.; Arakawa, H. In-Situ FT-IR Study on CO2 Hydrogenation over Cu Catalysts Supported on SiO2, Al2O3, and TiO2. *Appl. Catal., A* **1997**, *165*, 391−409.
(68) Fujita, S.-i.; Usui, M.; Ohara, E.; Takezawa, N. Methanol Synthesis from Carbon Dioxide at Atmospheric Pressure over Cu/ZnO Catalyst. Role of Methoxide Species Formed on ZnO Support. *Catal. Lett.* **1992**, *13*, 349−358.
(69) Fujita, S.; Usui, M.; Ito, H.; Takezawa, N. Mechanisms of Methanol Synthesis from CO2 and CO at Atmospheric Pressure over Cu−ZnO. *J. Catal.* **1995**, *157*, 403−413.
(70) Krastev, E. T.; Kuhl, D. E.; Tobin, R. G. Multiple Mechanisms for Adsorbate-Induced Resistivity: Oxygen and Formate on Cu(100). *Surf. Sci.* **1997**, *387*, 1051−1056.
(71) Dubois, L. H.; Zegarski, B. R. The Influence of Electron-Withdrawing Substituents on the Adsorption of CO on Copper. *Chem. Phys. Lett.* **1985**, *120*, 537−541.
(72) Nielsen, N. D.; Smitshuysen, T. E. L.; Damsgaard, C. D.; Jensen, A. D.; Christensen, J. M. Characterization of Oxide-Supported Cu by Infrared Measurements on Adsorbed CO. *Surf. Sci.* **2021**, *703*, 121725−121738.
(73) Safonova, O. V.; Guda, A.; Rusalev, Y.; Kopelent, R.; Smolentsev, G.; Teoh, W. Y.; Bokhoven, J. A.; Van; Nachtegaal, M. Elucidating the Oxygen Activation Mechanism on Ceria-Supported Copper-Oxo Species Using Time-Resolved X - Ray Absorption Spectroscopy. *ACS Catal.* **2020**, *10*, 4692−4701.
(74) Wang, X.; Rodriguez, J. A.; Hanson, J. C.; Gamarra, D.; Martinez-arias, A.; Fernandez-Garcia, M. In Situ Studies of the Active Sites for the Water Gas Shift Reaction over Cu−CeO2 Catalysts: Complex Interaction between Metallic Copper and Oxygen Vacancies of Ceria. *J. Phys. Chem. B* **2006**, *110*, 428−434.
(75) Rezvani, A.; Abdel-mageed, A. M.; Ishida, T.; Parlinska-wojtan, M.; Behm, R. J. CO2 Reduction to Methanol on Au/CeO2 Catalysts: Mechanistic Insights from De-Activation and SSITKA Measurements. *ACS Catal.* **2020**, *10*, 3580−3594.
(76) Lunkenbein, T.; Schumann, J.; Behrens, M.; Schlogl, R.; Willinger, M. G. Formation of a ZnO Overlayer in Industrial Cu/ZnO/Al2 O3 Catalysts Induced by Strong Metal-Support Interactions. *Angew. Chem., Int. Ed.* **2015**, *54*, 4544−4548.
(77) Kattel, S.; Ramírez, P. J.; Chen, J. G.; Rodriguez, J. A.; Liu, P. Active Sites for CO2 Hydrogenation to Methanol on Cu/ZnO Catalysts. *Science* **2017**, *355*, 1296−1299.
(78) Wu, P.; Yang, B. Significance of Surface Formate Coverage on the Reaction Kinetics of Methanol Synthesis from CO2 Hydrogenation over Cu. *ACS Catal.* **2017**, *7*, 7187−7195.
(79) Janse Van Rensburg, W.; Petersen, M. A.; Datt, M. S.; Van Den Berg, J. A.; Van Helden, P. On the Kinetic Interpretation of DFT-Derived Energy Profiles: Cu-Catalyzed Methanol Synthesis. *Catal. Lett.* **2015**, *145*, 559−568.
(80) Studt, F.; Behrens, M.; Kunkes, E. L.; Thomas, N.; Zander, S.; Tarasov, A.; Schumann, J.; Frei, E.; Varley, J. B.; Abild-Pedersen, F.; Nørskov, J. K.; Schlögl, R. The Mechanism of CO and CO2 Hydrogenation to Methanol over Cu-Based Catalysts. *ChemCatChem* **2015**, *7*, 1105−1111.

https://doi.org/10.1021/acscatal.1c00131
ACS Catal. 2021, 11, 4880−4892

(81) Zhao, Y. F.; Yang, Y.; Mims, C.; Peden, C. H. F.; Li, J.; Mei, D. Insight into Methanol Synthesis from CO2 Hydrogenation on Cu(111): Complex Reaction Network and the Effects of H2O. *J. Catal.* **2011**, *281*, 199−211.

https://doi.org/10.1021/acscatal.1c00131
ACS Catal. 2021, 11, 4880−4892